Weather and Climate Extremes 38 (2022) 100493

Contents lists available at ScienceDirect

Weather and Climate Extremes

journal homepage: www.elsevier.com/locate/wace

What causes a heavy precipitation period to become extreme? The exceptional October of 2018 in the Western Mediterranean

Samira Khodayar [a,*], Francisco Pastor [a], Jose Antonio Valiente [a], Pau Benetó [a], Florian Ehmele [b]

[a] Mediterranean Centre for Environmental Studies (CEAM), Valencia, Spain
[b] Institute of Meteorology and Climate Research (IMK-TRO), Karlsruhe Institute of Technology (KIT), Karlsruhe, Germany

ARTICLE INFO

Keywords:
Extreme weather
Heavy precipitation
Mediterranean
Large-scale conditions
SST
High-resolution modelling

ABSTRACT

The Mediterranean region is particularly exposed to heavy precipitation and flash flooding. Every autumn the region is affected by these weather-related hazards, frequently with immense costly and deadly consequences. What makes an already potentially damaging period in terms of heavy precipitation, even more intense? This is the underlying question in this study, in which the atmosphere and the ocean conditions in October 2018 are examined to identify anomalies favoring this intensification. Furthermore, the model representativity of the over-averaged precipitation period and underlying anomalies is analyzed across scales using climatological, seasonal, and event-based COSMO high-resolution model simulations.

Our investigation shows that October-2018, in the context of the climatological series from 1982 to 2018, could be marked as an unprecedented period because of the presence of intense and numerous low-pressure systems. Additionally, atmospheric moisture values placed this time above the climatological average, mainly for the high percentiles of the TCWV hourly anomalies. Specific humidity showed similar behaviour as TCWV except for pressure levels lower than 700 hPa, probably in relation to the evolution of the former Hurricane Leslie. The atmosphere-ocean interaction presented combined strong sea surface temperature (SST) and evaporation anomalies. April to October SST clearly exceeds climatological values while October-2018 presents both strong monthly anomaly and intense evaporation peaks preceding the most intense precipitation events. These large-scale features' anomalies were in general well captured by the high-resolution regional climate model simulations at climatic and seasonal scales leading to an accurate representation of accumulated precipitation for the October period. However, the numerical weather prediction simulations on an event scale revealed low predictability, in agreement with former investigations, due to differences at the location and intensity of the cut-off lows and particularly at the atmospheric moisture field.

The conclusions of this study show that it is not the most extreme period in terms of single anomalies which lead to extreme wet seasons, but the synergy of atmospheric and oceanic anomaly conditions with a constant interplay which made Autumn/October 2018 an extreme season/month.

1. Introduction

The western Mediterranean region (WMed) is frequently affected by heavy precipitation events (HPE) and flash flooding (Ferretti et al., 2000; Delrieu et al., 2005; Nuissier et al., 2011; Buzzi et al., 2014; Khodayar et al., 2021), especially during the autumn season. The densely populated coastal areas and the geomorphological characteristics of the region including a steep orography surrounding the WMed favour the mostly convective nature (Llasat et al., 2010) of HPEs in the region. The presence of small catchments promotes and aggravate flash floods. These events are characterized by their virulence and devastating socioeconomic impacts (Dobrovičová et al., 2015; Kron et al., 2019).

In addition to the presence of a favourable large-scale situation and low-level convergence (Homar et al., 2002; Romero et al., 1999; Martínez et al., 2008; Nuissier et al., 2011; Michaelides et al., 2018), the genesis of convection has been related to the moisture concentration and orography in the area (Pastor et al., 2010; Ehmele et al., 2015; Khodayar et al., 2018a). The warm Mediterranean Sea acts as a heat and moisture reservoir during late summer and early autumn (Pastor et al., 2001, 2015, 2018, 2020) from where low-level jets transport moisture and

* Corresponding author. Mediterranean Centre for Environmental Studies (CEAM), Parque Tecnológico, Charles R. Darwin Street, 14 46980, Paterna, Valencia, Spain.
E-mail address: khodayar_sam@gva.es (S. Khodayar).

https://doi.org/10.1016/j.wace.2022.100493
Received 26 January 2022; Received in revised form 15 July 2022; Accepted 10 August 2022
Available online 5 September 2022

instability towards the HPE areas (Duffourg and Ducrocq, 2011; Ricard et al., 2012; Khodayar et al., 2018b).

HPEs in the WMed concentrate in the months of September, October, and November (SON) with 75% of the major episodes occurring in this period (Insua-Costa et al., 2021). Hence, autumn months can be considered as the "extreme precipitation season" in the region. The high intensity of these periods could be a consequence of individual outstanding extreme precipitation events, the accumulated precipitation from multiple lower-intensity precipitation events, or a combination of both factors. The conditions leading to extreme wet seasons are still far from being completely understood in terms of underlying mechanisms and socio-economic impacts. Some recent research activities have been devoted to improving the understanding in terms of rainy seasons (e.g., Flaounas et al., 2021), demonstrating the complex interconnection between seasonal precipitation and synoptic-scale weather patterns, pointing out cyclones and warm conveyor belts as significant contributors to extreme wet seasons in most regions of the globe. In general, these investigations focus on a global scale and look into the responsible large-scale weather systems.

Different studies conducted in the last year's show an intensification of the water cycle at a global level. Durack et al. (2012) described the "rich get richer" mechanism explaining the intensification of the global water cycle from 1950 to 2000. This intensification was also described by Skliris et al. (2016) from observational data and climate projections. At a regional level, Mariotti (2010) identified an increase in evaporation in the Mediterranean since the mid-1970s primarily driven by SST increase. These trends in evaporation and SST could be a reason to drive the environmental conditions in the Mediterranean to be more prone to the development of HPE/extreme events in the context of climate change in the long term. But these feedback/intensification mechanisms present on the water cycle could also be part of shorter time scales leading to extreme precipitation seasons at regional scales. Thus, the accurate knowledge of the mechanisms behind these intense precipitation periods is of pivotal importance for better forecasting HPEs and to prevent their future potential damages. This is particularly relevant in a changing climate, in which future scenarios for the north-western Mediterranean (NWMed) project increased number and intensity of HPEs (Scoccimarro et al., 2016; Llasat, 2021; Tramblay and Somot, 2018).

This investigation intends to bring an insight into the atmospheric conditions and associated anomalies leading to the over-damaging wet autumn season of 2018 in the NWMed. In this period, Spain (Lorenzo-Lacruz et al., 2019), France (Caumont et al., 2021) and Italy (Davolio et al., 2020) were remarkably affected with devastating consequences, both from the economical point of view as well as the number of fatalities (Paprotny et al., 2018; Swiss, 2020). Furthermore, the model representativity of the intense rainy period is assessed across scales, at climatic, seasonal, and sub-seasonal, using high-resolution COSMO model simulations (Doms et al., 2013; Baldauf et al., 2011).

This study is structured as follows: Section 2 describes the data used and the methodology applied. Section 3 describes the autumn season of 2018 in terms of precipitation activity and Section 4 discusses the results focusing on the synoptic conditions, the atmospheric water vapour distribution and the SST and associated evaporation. Section 5 examines the model representativity across scales and conclusions are presented in Section 6.

2. Data and methods

2.1. Observations

2.1.1. CMORPH

CMORPH (Joyce et al., 2004) is a precipitation product produced at the Climate Prediction Center (CPC) throughout the Morphing Technique which uses passive microwave observations from low Earth orbit satellites and infrared data, subject to a bias correction with rain gauge measurements from the CPC over land and observations from the Global Precipitation Climatology Project (GPCP) over the ocean. Precipitation estimates are derived at a horizontal resolution of 8 km at the Equator and at a 30-min temporal resolution, covering the period from January 1998 to present at a global scale. In this study, precipitation estimates were downloaded for the period 2000–2019.

2.1.2. ERA5

ERA5 (Hersbach et al., 2020) is a comprehensive global reanalysis dataset, from 1979 to near real-time, which assimilates as many observations as possible in the upper air and near-surface. ERA5 reanalysis of the global weather and climate has been developed by the European Centre for Medium-range Weather Forecasting (ECMWF) under the auspices of EU-funded Copernicus Climate Change Service (C3S). For the present study, hourly geopotential and specific humidity data on pressure levels, as well as total column water vapour data, from 1982 to 2018 were accessed in the Meteorological Archival and Retrieval System (*MARS*) through the C3S Climate Data Store (CDS) facility (https://cds.climate.copernicus.eu/). The regular latitude–longitude grid (0.25° for the high-resolution deterministic reanalysis) on 37 pressure levels was selected, an interpolation post-processing conversion from the native reduced-Gaussian grid directly provided by the CDS facility. No-gaps consistent data could be collected for an extensive area, EU (21.5N–62.5N, 45.0W-40.0E), in order to obtain a coherent representation of our regional system.

2.1.3. Sea surface temperature and ocean evaporation

For the study of sea surface temperature, we have used data from the National Centers for Environmental Information. 2020. Daily L4 Optimally Interpolated SST (OISST) In situ and AVHRR Analysis Version 2.0 PO.DAAC, dataset accessed 2021-02-01 at https://doi.org/10.5067/GHAAO-4BC02 (Reynolds et al., 2007). AVHRR_OI is a blended SST data set covering the Mediterranean region with a smoothed and complete field at 0.25° spatial resolution with daily data available from September 1981 up to the present. Extensive information and descriptions of the data set can be found in Banzon et al. (2016) wherein the authors state its suitability for climate analysis.

In the case of evaporation, we have used the Objectively Analyzed air-sea Fluxes (OAFlux) for the Global Oceans project data set (Yu and Weller, 2007). This dataset provides data for different air-sea fluxes and variables from which we have selected moisture flux (ocean evaporation). OAFLUX data covers the entire globe with 1° spatial resolution and offers monthly data from 1958 to 2018 and daily data since 1985. In our study, we have used monthly data as our intention was to produce a long enough climatology of evaporation in the Mediterranean region.

2.2. Modelling: COSMO and COSMO-CLM

The simulations used in this study are performed with the non-hydrostatic Consortium for Small-Scale Modeling (COSMO) model (e.g., Doms et al., 2013; Baldauf et al., 2011) in version 5.0. Three different types of simulations are done: a climatological run (CLIM) covering the years 1999–2018 (the first year 1999 is treated as spin-up), a seasonal run (SS) covering the period from September 1 to October 31, 2018, and event simulations (EV) for each of the investigated episodes covering only a short time frame from hours to few days (Table 1). The climatological and seasonal simulations are run in the climate mode of the COSMO model (COSMO-CLM) using the CLM version 15 (e.g., Rockel et al., 2008). The episodic simulations are run in NWP mode (numerical weather prediction). While in NWP mode the slow-changing variables like SST, plant cover, and others are kept constant over the simulation period, they are updated regularly in COSMO-CLM.

For all three simulation types, a 7 km and a 2.8 km horizontal resolution were used. The 7 km runs are forced using hourly ERA5 reanalysis data. The simulation domain covers Western and Central Europe and a large area of the North Atlantic (Fig. 1). Both shallow and deep

Table 1
Model characteristics (Part 1) of the long-term climate run (CLIM), the seasonal simulations (SS), and the episodic simulations (EV) performed with the COSMO model. CLIM and SS are run in climate mode (COSMO-CLM), while EV 1–3 are run in NWP mode.

Simulation	Resolution	Initial & Boundary Conditions	Start-end of the simulation period	Duration	Latitude range, Longitude range	Vertical levels	Integration time step
CLIM	0.0625° ~7 km	ERA5	01/01/1999 00 UTC	20 y	25.9°N – 61.1°N 32.8°W – 36.3°E	50	60 s
	0.025° ~2.8 km	CLIM 7 km	– 01/01/2019 00 UTC		33.0°N – 46.9°N 14.4°W – 6.1°E	60	20 s
SS	0.0625° ~7 km	ERA5	01/09/2018 00 UTC –	61 d	19.5°N – 59.9°N 50.6°W – 37.0°E	50	60 s
	0.025° ~2.8 km	SS 7 km	01/11/2018 00 UTC		31.5°N – 50.0°N 16.0°W – 21.9°E	60	20 s
EV1-MALL (ES)	0.0625° ~7 km	ERA5	08/10/2018 18 UTC –	36 h	21.3°N – 58.8°N 48.7°W – 34.8°E	50	60 s
	0.025° ~2.8 km	EV1-MALL 7 km	10/10/2018 06 UTC		31.5°N – 50.0°N 16.0°W – 21.9°E	60	20 s
EV2-AUD (FR)	0.0625° ~7 km	ERA5	13/10/2018 18 UTC –	48 h	21.3°N – 58.8°N 48.7°W – 34.8°E	50	60 s
	0.025° ~2.8 km	EV1-AUD 7 km	15/10/2018 18 UTC		31.5°N – 50.0°N 16.0°W – 21.9°E	60	20 s
EV3-VAIA (NI)	0.0625° ~7 km	ERA5	26/10/2018 06 UTC –	114 h	21.3°N – 58.8°N 48.7°W – 34.8°E	50	60 s
	0.025° ~2.8 km	EV1-VAIA 7 km	31/10/2018 00 UTC		31.5°N – 50.0°N 16.0°W – 21.9°E	60	20 s

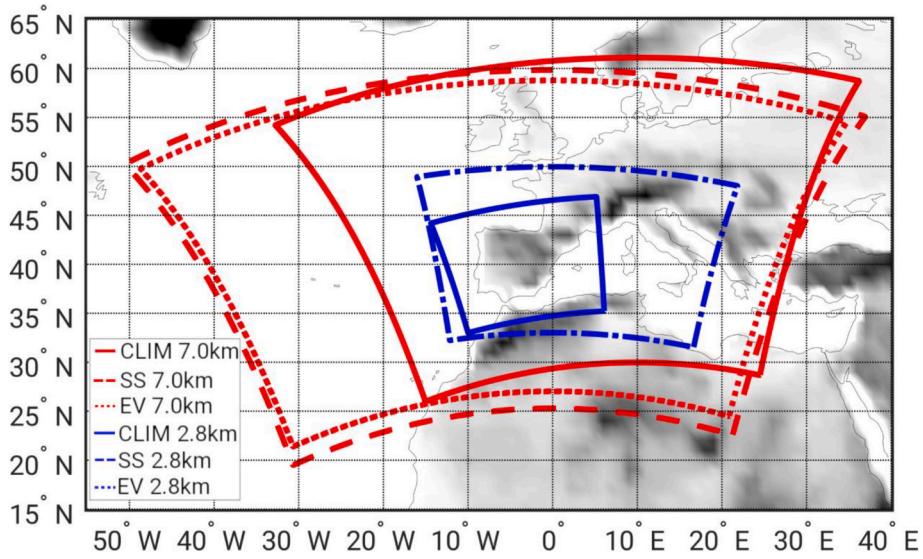

Fig. 1. Simulation domains for the 7 km (reddish) and 2.8 km (blueish) COSMO simulations.

convection are parameterized using the convection scheme of Tiedtke (1989). The 7 km runs are then used as forcing for the 2.8 km simulations. The simulation domain of the 2.8 km simulations mainly covers the Iberian Peninsula and the western Mediterranean region. Only shallow convection is parameterized in this case with the Tiedtke (1989) scheme. An overview of the model setup, physics, and parametrizations is given in Tables 1 and 2. In all cases, no further data assimilation was applied.

For the episodic simulations, the simulation periods are selected based on hourly observed CMORPH precipitation (Joyce et al., 2004) spatially averaged over the investigation domains of the corresponding event. First, the timing of the maximum precipitation (peak) is extracted. Second, we look for the point in time when the precipitation starts to increase towards this peak (reference point RP1) and also for the time when the decrease after the precipitating peak ends (reference point RP2). In the case of multiple peaks within 24 h, the last peak is used to estimate RP2. The starting point of the simulation then is 18h prior to RP1 to have a spin-up of 6h followed by 12h of simulation time almost unaffected by boundary effects. With respect to a possible shift in time of the simulated precipitation event, the ending of the simulation is 6h after RP2 (Table 1). Doing so, there should be enough buffer to fully capture the events.

The single events investigated affect in particular the Balearic island of Palma de Mallorca in Spain on the 9 to 10 October 2018 (EV1(event): MALL, ES), the Aude region in France on the 14 to 15 October 2018 (EV2:AUD, FR), and north and north-eastern Italy on the 27 to 29 October 2018 (EV3:Vaia, NI).

2.3. Methodology

To assess the precipitation conditions during the autumn season and particularly the October period of 2008, the climatological anomaly was calculated using 90-60-30 day windows using ERA5 precipitation observations for the whole period under investigation. Following Flaounas

Table 2
Model characteristics (Part 2) of the long-term climate run (CLIM), the seasonal simulations (SS), and the episodic simulations (EV) performed with the COSMO model. CLIM and SS are run in climate mode (COSMO-CLM), while EV1-3 are run in NWP mode.

Simulation	Resolution	Convective scheme	PBL scheme	Radiative scheme	Microphysical scheme	Soil scheme
CLIM	0.0625° ~7 km	Deep and shallow (Tiedtke, 1989)	second-order TKE closure at hierarchy level 2.0 (Mellor and Yamada, 1974). Prandtl-layer: stability and roughness- length dependent surface flux formulation (Louis, 1979)	Ritter and Geleyn (1992): delta-two-stream radiation scheme; short and longwave fluxes (employing eight spectral intervals); full cloud-radiation feedback.	Cloud water condensation and evaporation by saturation adjustment. Precipitation formation by a bulk microphysics parameterization including water vapour, cloud water, cloud ice, rain and snow with 3D transport for the precipitating phases (Doms et al., 2013).	TERRA-ML (Jacobsen and Heise, 1982; Doms et al., 2013)
	0.025° ~2.8 km	Only shallow (Tiedtke, 1989)				
SS	0.0625° ~7 km	Deep and shallow (Tiedtke, 1989)				
	0.025° ~2.8 km	Only shallow (Tiedtke, 1989)				
EV1-3	0.0625° ~7 km	Deep and shallow (Tiedtke, 1989)				
	0.025° ~2.8 km	Only shallow (Tiedtke, 1989)				

et al. (2021), an extreme wet season stands for the 90-days period with the largest accumulated precipitation in the last 40 years, whereas a secondary extreme season is the 90-days period that exhibits at least 90% of accumulated precipitation of the primary extreme season.

The large-scale synoptic situation and the atmospheric water vapour content as well as the SST and associated evaporation are investigated to assess the atmospheric and Mediterranean Sea conditions and to identify possible anomalous behaviour during October 2018.

Synoptic conditions involved during October 2018 were investigated and put in correlation to the historic rest of the 1982–2018 Octobers. Specifically, geopotential heights, downloaded through the C3S-CDS facility (Hersbach et al., 2018), for ERA5 hourly data, on different pressure levels (300, 500, 700, 850, 950 and 1000 hPa) at 0.25° spatial resolution were investigated. A percentile analysis was performed on each dataset that featured a whole month of geopotential heights for each of the 0.25° grid points. As a result, for each of the pressure levels, 21 percentile maps were obtained for each of the 37-year Octobers: one map for each geopotential percentile ranging from 0th to 100th in 5th steps. 2D distributions of climatological means for each of the geopotential percentiles were obtained through the average of the 1982–2018 Octobers at 0.25° spatial resolution. In this manner, quantification of the anomalies was performed by subtracting each climatological mean distribution from its corresponding geopotential percentile map. In the particular case of these geopotential maps, a large region of interest (ROI) was defined (EU: 21.5N–62.5N, 45.0W-40.0E). In addition, different ROIs have been further defined in relation to other atmospheric variables: total column water vapour, SST and evaporation fluxes' calculations (Fig. 2).

As HPEs must be fuelled with atmospheric water vapour available, total column water vapour (TCWV) fields from the ERA5 hourly dataset were also considered for the analysis. These fields were transformed into probability density functions (PDF) as TCWV frequency distributions for

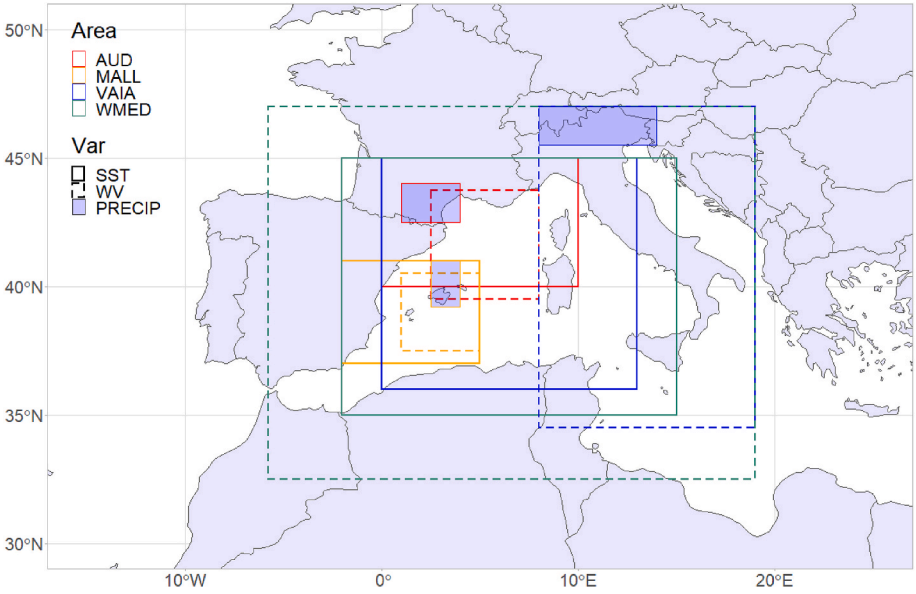

Fig. 2. Analysis areas for SST and evaporation (solid lines), total column water vapour (dashed lines) and CMORPH precipitation (shadowed boxes) covering WMed and the HPE events' areas in October 2018.

different ROIs, considered as the atmospheric moisture recharge areas for each of the precipitation events that took place during October 2018. All these ROIs, besides containing the 3 localizations of the main precipitation events during the October 2018 period, take into account a large sea area where moist air masses develop: EV-MALL (ES): 40.5N–37.5N, 1.0E-5.0E; EV-AUD (FR): 43.75N–39.5N, 2.5E-8.0E; and EV-VAIA (NI): 46.5N–34.5N, 8.0E-19.0E (Fig. 2).

Considering each of the ROIs, for each of the 1982–2018 Octobers containing hourly TCWV fields, a PDF can be estimated, and the average of the outcome series of PDFs over the 1982–2018 period be considered as the climatological average PDF for the whole 37-year period. In a similar way as anomalies are calculated, a PDF difference between the distribution associated to October-2018 and the climatological average will provide information on TCWV extremes for that month and specific ROI. Furthermore, for the examination of the SST and the evaporation fluxes using satellite data new ROIs are defined (Fig. 2). This is to consider the contribution of water vapour to the atmosphere from the areas near the precipitation localization, avoiding those areas not directly intervening in the HPE, also the moisture recharge of the air mass along its path over the sea for at least 48 h prior to the precipitation event. To this end, air mass near-surface trajectories have been computed with HYSPLIT (not shown).

3. October 2018 and the "Mallorca", "Aude" and "Vaia" events

The CMORPH 2018 October accumulated precipitation anomaly against the 2000 to 2019 climatology presents monthly precipitation well above the corresponding climatology for most of the western Mediterranean region (Fig. 3a). Specifically, anomalies are observed along the northern coast of the western Mediterranean, from the Gulf of Valencia to the Gulf of Genoa, as well as in northern and southern Italy, with precipitation accumulations between 100 and 300 mm above the climatological monthly mean. This indicates that October of 2018 could be identified as an extreme wet month with a monthly average value of 24 mm above the climatological mean for the 95th percentile (Fig. 3b). Besides, anomalies exceed 30 mm in the last two weeks of the month highlighting the importance of the extreme precipitation events that occurred during this period.

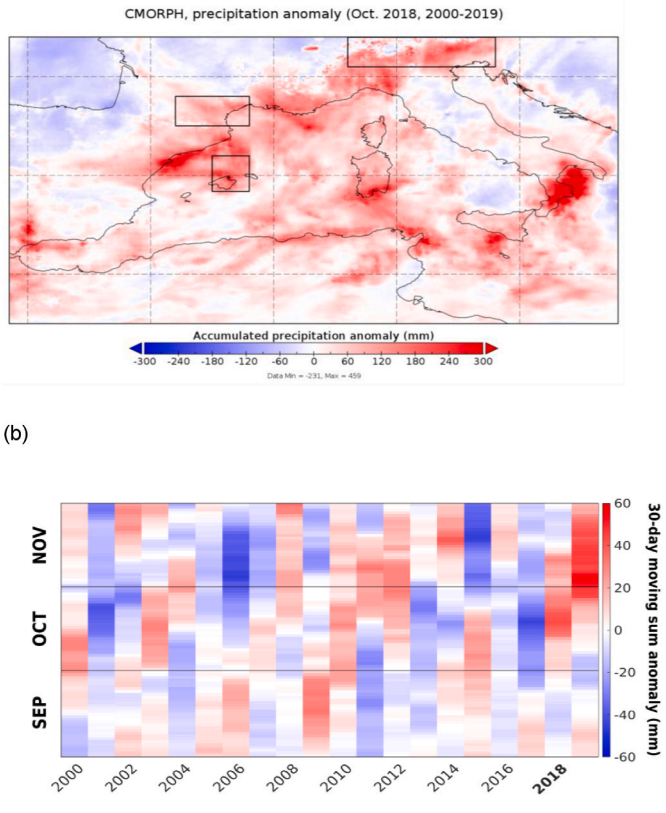

Fig. 3. (a) Spatial distribution of the precipitation anomaly for October 2018 with respect to the 2000–2019 CMORPH climatological values in the WMed. Black boxes locate the investigation domain for each event. (b) Climatological temporal anomaly ("wet month 30 day moving window") for the 95th percentile using CMORPH observations within the WMed.

Individual outstanding extreme precipitation events characterize the period affecting the WMed. Among them, three periods stand out because of the intensity of precipitation and the damage inflicted in the affected areas. These cases affect in particular the Balearic island of Palma de Mallorca in Spain on the 9 to 10 October 2018 (EV1:MALL), the Aude region in France on the 14 to 15 October 2018 (EV2:AUD), and north and north-eastern Italy on the 27 to 29 October 2018 (EV3:VAIA). These events have been individually described in detail in the literature, nevertheless, a brief description is given in the following.

Torrential rain during the afternoon of October 9th, 2018, in the north-east of Mallorca island resulted in flash floods leading to 13 fatalities and severe economic damage (Lorenzo-Lacruz et al., 2019). A cut-off low centered to the east of the Iberian Peninsula, and a weak easterly flow over the western Mediterranean Sea characterized the synoptic scale and low-level atmosphere during this episode. Convective cells initiated over the sea to the east of the island and penetrated Mallorca successively resulting in heavy and persistent rain. Precipitation records over 200 mm were measured at several stations with most of the precipitation registering between 16:00 and 22:00 LT. The operational forecasting tools and services were in this case unable to predict the devastating situation showing a remarkable underestimation of accumulated precipitation in the affected region.

On 14 and 15 October, the Aude watershed in south-western France was affected by heavy precipitation leading to severe flash flooding (Caumont et al., 2021). Up to about 300 mm of rain in 11 h were produced by a back-building quasi-stationary mesoscale convective system. This was a "typical" Mediterranean HPE following a classic synoptic situation, in which the former Hurricane Leslie was involved in the formation of a Mediterranean surface low. The presence of a former hurricane and the positive Mediterranean SST anomaly were shown to contribute to the severity of the case (Mandement and Caumont., 2021). The event showed limited predictability given the small size of the watersheds affected.

On 27–29 October, a very intense precipitation and windstorm event affected the eastern Italian Alps (Giovannini et al., 2021). Up to 850 mm accumulated in the three days period of the event. On the synoptic scale a trough over the eastern Atlantic extending to France and Spain characterized the situation, while at the surface a wide cyclonic area over the WMed moved towards northwestern Italy. This event was well predicted regarding the well-defined large-scale forcing, also the complex local scale features. However, total precipitation amounts were significantly underestimated.

4. Atmospheric and Oceanic anomalies in the western Mediterranean for the October 2018 conditions

4.1. Synoptic situation and atmospheric water vapour content

Synoptic conditions leading to extreme precipitation at coastal locations in the western Mediterranean are mostly characterized by upper-level cut-off lows filled with cold air that can remain nearly stationary for days or even move westward opposite to the general flow (Ferreira, 2021). During October 2018, several cut-off cyclones travelled throughout the Mediterranean region. On October 7, a cut-off depression emerged from a sharp mid-tropospheric trough offshore the west coast of France and moved southwest quickly. It centered at the east of the Iberian Peninsula on October 9, producing heavy precipitation on its easterly flank, especially at the south-eastern part of Mallorca Island. As

soon as the depression moved westward, it was re-included in the upper-level main flow in the afternoon of October 10. On October 13, extratropical cyclone Leslie impacted Portuguese coasts, pulled by an Atlantic sharp trough, with its remnant core crossing the Gulf of Biscay. The strong associated vorticity led upper-level cold air to be advected over the Balearic Sea south of the Pyrenees. Additionally, a long airmass tail associated with extratropical cyclone Leslie could be identified to be incorporated over the Balearic Sea through the Gibraltar Strait and Alboran sea. The heaviest precipitation occurred during the night from October 14 to 15 in southern France, while the cold depression moved southeast into the WMed. On October 18, a new upper-level cut-off low formed from an Atlantic trough and positioned quickly to the Strait of Gibraltar, creating a wide easterly flow at the Mediterranean region, resulting in heavy and prolonged precipitation leading to an HPE episode in the eastern coast of the Iberian Peninsula. The cut-off depression extended over the Gulf of Cadiz, moving westward first and then northwest to the southern coasts of Portugal on October 20 and finally leading to an extreme precipitation event on October 21 at Malaga province in the south of Spain. In the evening of October 27, a broad trough developed towards the south reaching the entire Iberian Peninsula, even further to northern Africa. On its easterly flank, cyclogenesis formed a deep low in the Gulf of Genoa for the next 2–3 days, after which, it moved northward advecting copiously moist air masses over the Northern Italy region and producing two heavy and consecutive precipitation events.

From a descriptive approach using ERA5 information, October 2018 was characterized by many low-pressure air masses that detached from the northern zonal circulation and affected the Western Mediterranean region. The 5th and 95th 300 hPa geopotential percentile anomalies are provided in Fig. 4 for October 2018 as a 2D-map centered at the Iberian Peninsula (additional Figure A1 provided in the Appendix for the 500 hPa level). Although not shown, it was recognised that 300 hPa pressure level better captured the geopotential anomaly differences in our region of interest. Geopotential negative anomalies for the 5th percentile are observed for the whole Iberian Peninsula and part of the Western Mediterranean, denoting an anomalous low-pressure synoptic condition for October 2018. Additionally, the 2D-spatial distribution associated with the 95th percentile shows no anomalies at the Iberian Peninsula region, but positive anomalies at high latitude regions, indicating an above normal high-pressure temporary condition at that zonal region.

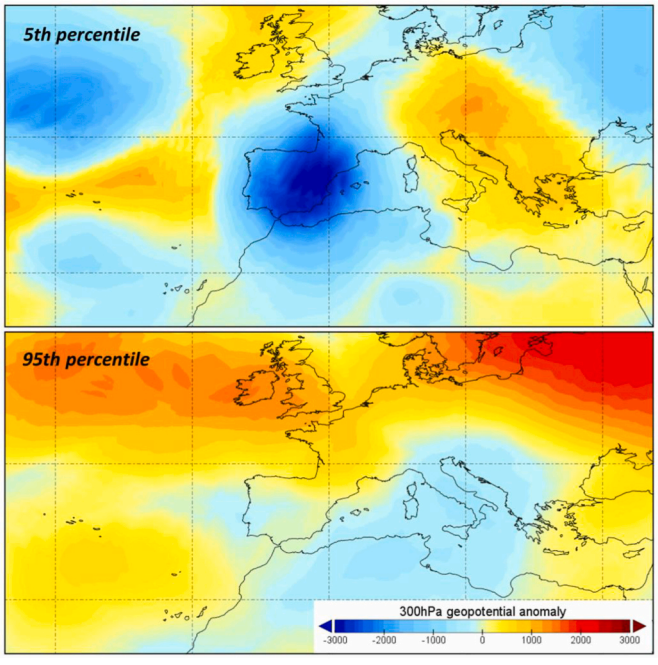

Fig. 4. Spatial distribution of the 300 hPa geopotential anomalies (in m^2s^{-2}) for the 5th and 95th percentiles at 0.25° latitude/longitude resolution centered at the Iberian Peninsula for October 2018, each based on their respective climatological percentile mean for the period 1982–2018.

At a defined ROI centered at the Iberian Peninsula (IP: 34.5N–44.5N, 10.0W-5.0E), spatial averages of anomaly scores and climatological means were estimated for each ith 300 hPa geopotential percentile. The ratio of both spatial averages provided a percentage value of the anomaly for the ROI in question. Fig. 5 contains these anomaly percentages as a heatmap, where red cells associated with the lowest geopotential percentiles can be related to monthly synoptic situations that are relatively dominated by blocking highs over the region of interest IP, i.e., atmospheric anticyclonic fields that block or divert the common path of cyclones and troughs towards the Iberian Peninsula for this time of the year. On the contrary, blue cells associated with the lowest geopotential percentiles can be connected to more abundant than usual cut-off lows that mostly emerge from an Atlantic trough and make their way to the Iberian Peninsula. As a general rule, the more positive (negative) these anomaly percentages associated with the lowest percentiles, the greater the number and intensity of the blocking highs (cut-off lows) above normal. As seen from the heatmap, October 2018 shows the greatest number and deepest detached lows for the climatological period considered, reaching the anomaly percentage negative values around 3% and 2.4% for the 0^{th} and 5th 300 hPa geopotential percentiles, respectively. These values conformed to an unprecedented situation not found previously in the climatological period from 1982 to 2018. The second October in the ranking of negative anomaly percentages corresponded to 2008, for which extreme precipitation conditions were also reported (SAIH, Automatic System of Hydrological Information, http://saih.chj.es/chj/saih/) at the Mediterranean Iberian Peninsula from October 9th to 12th.

Furthermore, red cells corresponding to the highest and intermediate geopotential percentiles can be related to a predominance of high-pressure air masses over the region of interest IP, that can be translated into relatively strong anticyclones or persistent and elongated ridges aloft more frequently than usual. On the contrary, blue cells corresponding to the intermediate geopotential percentiles can be connected to sustained relatively low atmospheric pressure conditions that are more frequent than usual, extending as troughs aloft over large areas of continental Europe. White cells of the heatmap denote geopotential percentiles that meet the average synoptic conditions represented by the climatological mean for the period 1982–2018. It is also remarkable how anomalies linked to the intermediate and highest geopotential

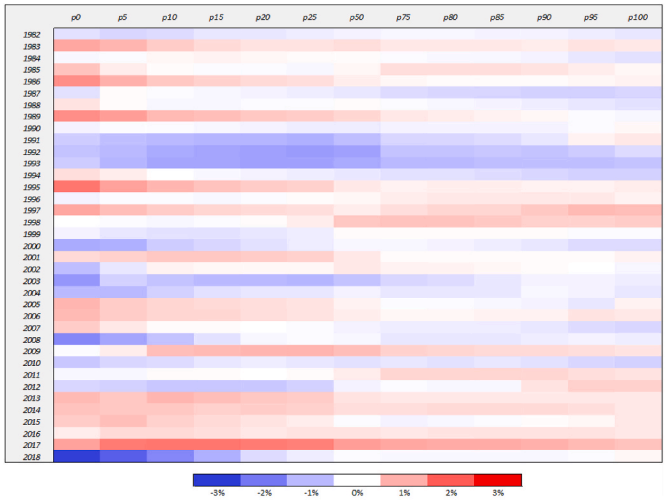

Fig. 5. Heatmap of anomaly percentages (climatological mean normalised anomalies) for each of the 1982–2018 Octobers, the Iberian Peninsula region and for a selected set of 300 hPa geopotential percentiles.

percentiles for October 2018 were irrelevant, indicating typical high pressure air masses over the Iberian Peninsula for this particular month of the series.

Total column water vapour (TCWV) fields from the ERA5 hourly dataset were also considered to construct PDF time series for the defined ROIs and for the WMed area. Fig. 6 shows the time series of the TCWV PDF difference between each of the ROI October-2018 and the climatological average. Positive (negative) values for the PDF difference denote TCWV values for which October-2018 PDF marks above (under) the climatological average PDF. This climatological average leads to a wide-spread distribution shape since it contains a very large number of heterogeneous air masses for the 37-year period considered. As seen from the positive values in PDF difference, the smaller (larger) the ROI size, the narrower (wider) shape of its associated PDF, denoting a more homogenous (heterogenous) air mass. From the negative values in PDF difference, an evident wide distribution shape is always observed, displaying the range where the climatological average PDF runs through the October month, showing at the same time its dependence on the day of the month (DOM). The figure shows how the frequency of moist air masses rises before and during each of the HPE at their associated ROI with respect to the climatological average. For the whole WMed, moist air masses are more frequent than the average October, represented by the broad blue strip that denotes the position for the 37-year climatological average.

In order to analyse hourly anomalies for the TCWV fields in a ROI, the median of the 37-year climatological average PDF was determined hourly, since it is not exactly constant throughout the October month but decreases slowly from the beginning to its end. For each grid point in the WMed region, hourly anomalies for TCWV were derived by subtracting the obtained median from the hourly TCWV fields. Fig. 7 shows the resulting statistical analysis as a time series boxplot of these hourly anomalies for the 1982–2018 Octobers in the WMed region. Some of the highest and lowest percentiles of the hourly anomalies, as well as their maximums and minimums for all the Octobers, are also plotted as whiskers marks. Although not outstanding in the 37-year period, October 2018 contains a great number of positive hourly anomalies, being their highest percentiles in a high ranking of the October series. It is remarkable how a positive climatological trend can be encountered for the high percentiles in the October series, the higher the percentile, the larger the trend. In contrast, for the low percentiles, a linear regression of their time series results in a negligible trend. A larger positive (negligible) trend for the high (low) percentiles may indicate a 37-year period tendency for the moist air masses to become moister and for the relative dry air masses to stay on the same moisture levels. Therefore, October 2018 can be considered as a month above the average for atmospheric moisture content, precisely around 7.3% (6.5%) moister for its 50th (94th) percentile of the TCWV hourly anomalies. For each percentile, this anomaly percentage is a normalised measure of the excess (lack) of moisture above (under) an average, and it is estimated as the difference between the percentile value and the average of the October percentiles series normalised by its 37-year-period TCWV absolute mean value. Large TCWV anomaly percentages for the highest percentiles of hourly anomalies may be considered as an additional ingredient for the onset of HPEs.

A similar analysis can be done for the specific humidity (SH) fields for each of the pressure levels (500, 700, 850, 950 and 1000 hPa) that were selected, taken each level independent of the other. In this sense, hourly anomalies for the SH fields associated with each pressure-level were calculated in relation to their 37-year climatological average PDF in a similar process as done with the TCWV fields for the WMed region. Again, a time series boxplot of the hourly anomalies was done for each of the pressure levels, and a statistical analysis was performed on the highest and lowest percentiles. Positive climatological trends were also encountered for the high percentiles in each of the October series, in a similar way as that found for the TCWV hourly anomalies. SH anomaly percentages were estimated in a process following the same procedure as described above. Fig. 8 joins the previously obtained TCWV anomaly percentages and the currently estimated SH anomaly percentages for each of the pressure levels that were considered in a line graph for the October 2018 and WMed region. As seen from the figure, the moistest pressure level above the average would correspond to the 700 hPa layer, the anomaly percentages displaying an enlargement as level pressure

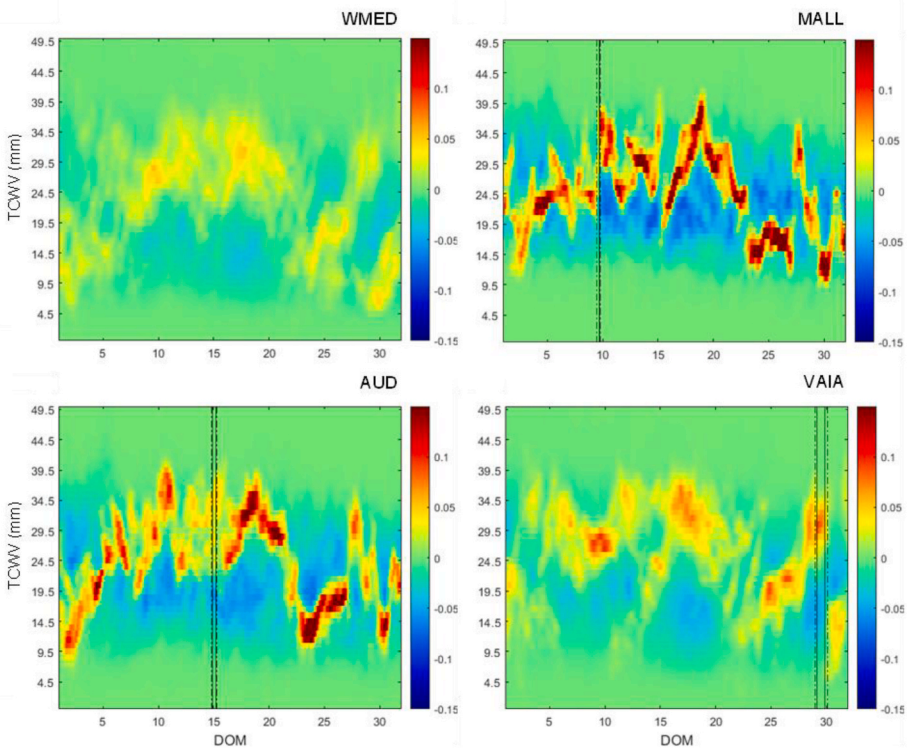

Fig. 6. Time series of the differences between probability density functions, PDFs, calculated as the hourly frequency normalised distributions of total column water vapour (TCWV) associated to 12h-running periods minus the climatological frequency average distribution for the 1982–2018 period. PDFs differences are for October 2018 and for several recharge regions of interest: the Western Mediterranean Basin (WMed), Mallorca (MALL), Aude region (AUD) and North Italy (VAIA). The onset and ending of each respective (high) precipitation event are marked with a dash (solid) line.

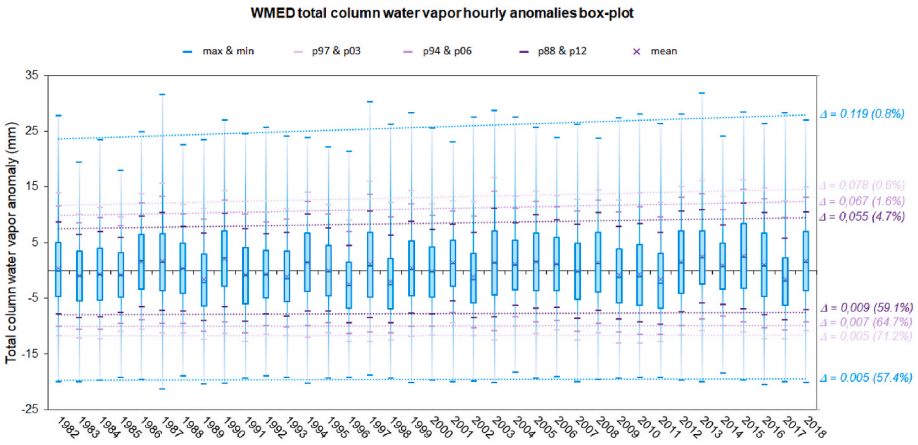

Fig. 7. Time series boxplot showing main features of the probability density functions associated with total column water vapour hourly anomalies (mean, median, quartiles, several percentiles and maximum and minimum) for WMed during the Octobers from the 1982–2018 period. Period trends for the different percentiles and maximum and minimum values are represented as straight lines with their respective slopes (Δ).

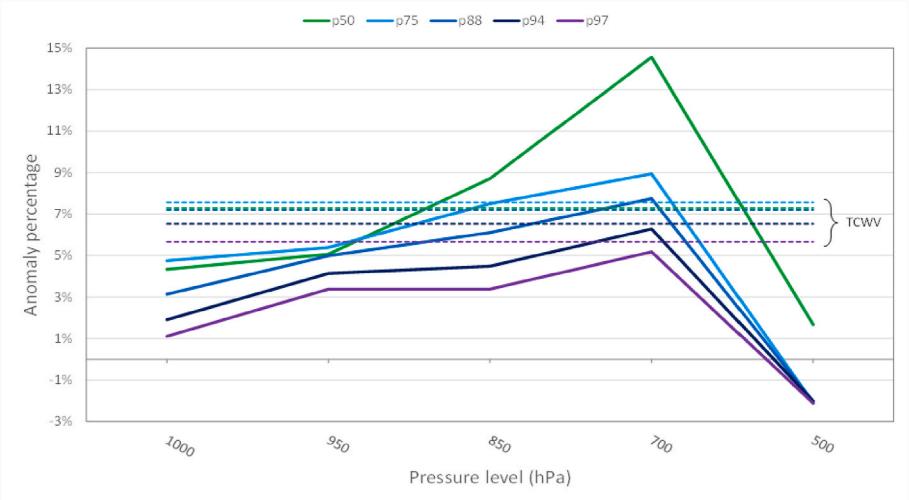

Fig. 8. For the WMed region, TCWV and SH anomaly percentages obtained for October 2018 for a selected set of pressure levels and some high percentiles. TCWV anomaly percentages are represented as horizontal lines only for comparison purposes.

increases until attaining their lowest values (negative) at 500 hPa.

4.2. Sea surface temperature and evaporation

Among many other mesoscale features, the Mediterranean Sea plays an important role in both the water cycle and/or the genesis and development of HPE events in the Mediterranean region. Fig. 9a shows the 2018 mean daily WMed SST compared with the 1982–2018 mean climatology. Western Mediterranean SST in 2018 was clearly above the climatic mean from most of April until the end of October with especially high values in August and September when SST values exceeded the standard deviation values in the basin, probably leading to a huge energy accumulation in the WMed area. Regarding evaporation, larger variability for daily values in 2018 than in the case of SST can be seen in Fig. 9b. It is noticeable the presence of some peak evaporation events in or around October. Two major evaporation events can be seen during the last days of September and the start of October that importantly exceed the standard deviation values, with a significant contribution of moisture to the atmosphere. Another two smaller but significant events can be seen during the month while the highest evaporation event occurred at the end of October, starting on October 25 and with its maximum on October 30.

The same analysis was run for the HPE events of Aude, Mallorca and Vaia areas (additional Figures A3, A2, A4 provided in the Appendix). In all three cases, SST for the studied regions showed the same behaviour of the WMed basin with values exceeding standard deviation in August and September and values above climatic mean during October (not shown). Regarding evaporation in the HPE areas, in all three cases, intense evaporative events could be seen preceding the precipitation event period.

To better signal October 2018 *"extraordinary"* character time series of monthly anomalies for SST and evaporation in the WMed basin were computed, shown in Fig. 10. As expected from Fig. 9, August value of SST anomaly clearly exceeded the 75th percentile while September 2018 shows the highest anomaly for this month in the complete 1982–2018 period. Regarding evaporation anomalies, October 2018 presents a very high positive anomaly also substantially greater than the 75th percentile. To gain perspective of the actual character of October 2018 a composite of SST and evaporation anomalies is shown in Fig. 11.

In Fig. 11 October 2018 is in the *warm-wet* quadrant, in the same way as in other October months. While there are years, such as 2014, that show very high SST anomalies, but no notable anomaly in terms of evaporation, on the contrary, a year such as 2003 shows a strong positive evaporation anomaly but an almost neutral SST one. October

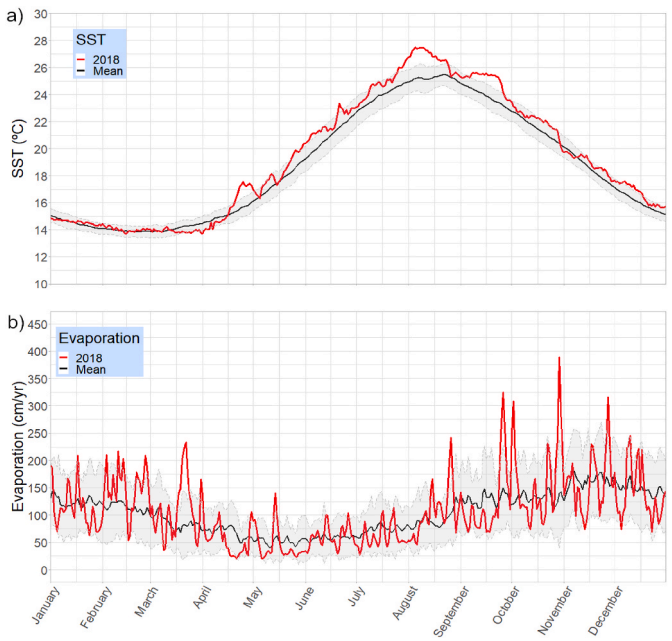

Fig. 9. (a) SST and (b) evaporation, annual cycle in the WMed region. Black line denotes the daily mean value for the 1982–2018 period for SST and 1985–2018 for evaporation. Red line shows mean daily values for 2018. Grey shadowed band shows the standard deviation in both cases. (For interpretation of the references to colour in this figure legend, the reader is referred to the Web version of this article.)

months in years such as 2009, 2011, 2016 and 2018 show a noticeable combination of high monthly anomalies, although not the highest ones, for both SST and evaporation.

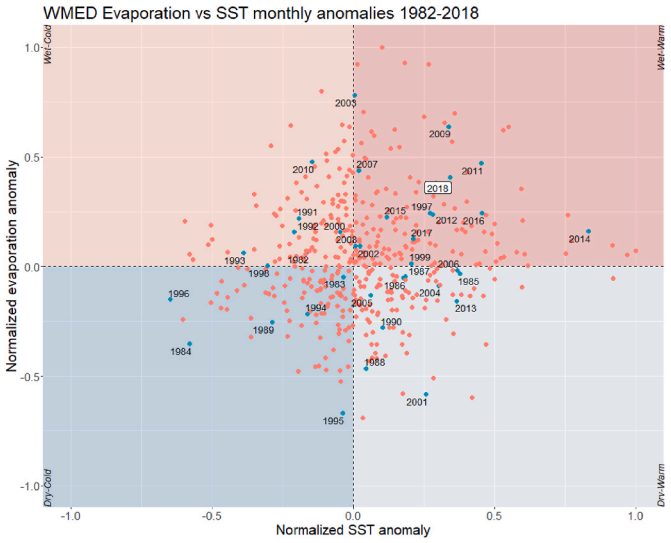

Fig. 11. Evaporation vs SST monthly anomalies (1982–2018). Each circle denotes a month, blue dots represent October for each year in the series. (For interpretation of the references to colour in this figure legend, the reader is referred to the Web version of this article.)

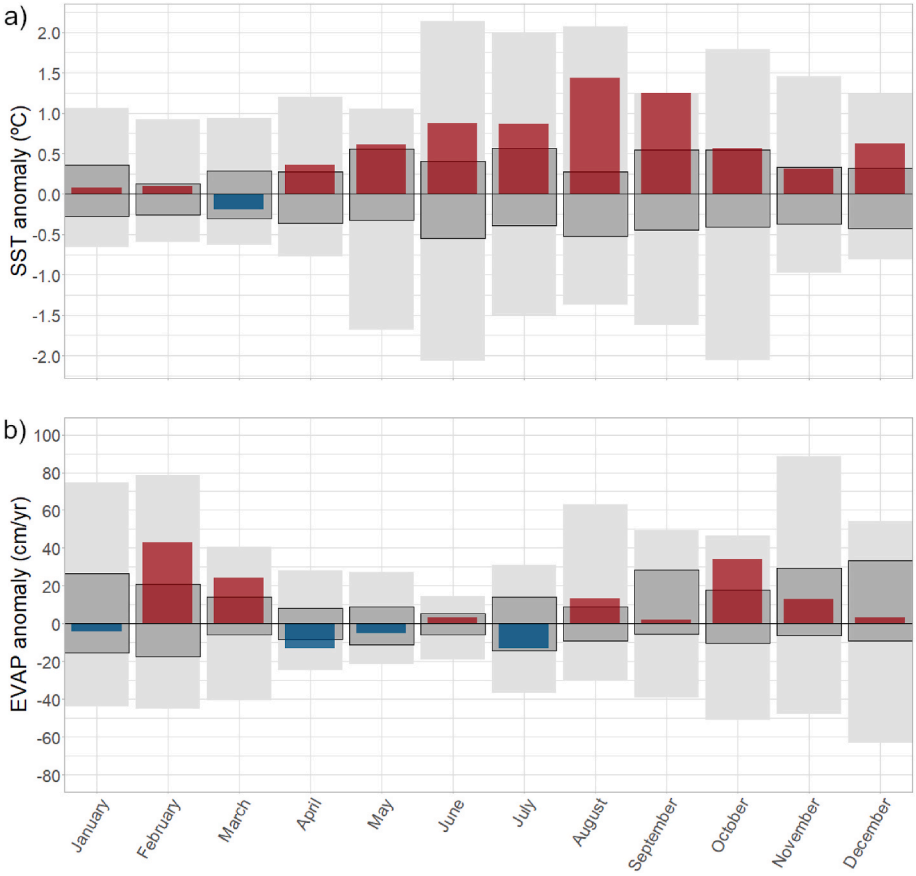

Fig. 10. (a) SST and (b) evaporation 2018 monthly anomalies (red for positive values and blue for negative ones). Light grey box span for the minimum-maximum values of the anomaly series 1982–2018 and dark grey box stands for the 25th-75th percentile interval. (For interpretation of the references to colour in this figure legend, the reader is referred to the Web version of this article.)

5. Model representativity across scales

The model representativity of the October 2018 conditions regarding accumulated precipitation and previously identified anomalies is examined at climatic, seasonal, and sub-seasonal scales. The performance of the climatic and seasonal suite of simulations well represents the monthly mean of the accumulated precipitation (Fig. 12a), the anomaly large-scale conditions, the total column water vapour anomaly as well as the positive evaporation anomaly (Fig. 13).

Despite a slight underestimation of the accumulated precipitation at the CLIM simulation, this as well as the SS simulation capture each one of the extreme precipitation events during October 2018, although with differences with respect to observations. Differences less than 2% regarding typical geopotential variations at 500 hPa are identified (Fig. 13a). Differences between CLIM and ERA5 anomalies as well as SS and ERA5 anomalies for percentile 5th are very similar to percentile differences regarding magnitude and spatial distribution. Total column atmospheric moisture anomaly differences between CLIM and SS simulations and ERA5 are in general less than 10% (Fig. 13b). Both CLIM and SS simulations reveal, in relation to ERA5, a slight overestimation over the WMed, whereas the CLIM simulation is drier over the Atlantic in comparison with the SS simulation showing a greater anomaly. This could be in relation to the different representations of former extratropical cyclone Leslie, which enters later from Portugal on the SS simulation, relevant in terms of its role as supplier of moisture during the extreme precipitation periods (Mandement and Caumont, 2021). An increased moisture advection to the Mediterranean region caused by the interaction of former tropical cyclones was discussed by Pinto et al. (2013). Monthly mean evaporation from sea surface and anomalies over the WMed are also well captured in the CLIM and SS simulations (Fig. 13c). In all model realisations greater evaporation is found over the WMed and Atlantic Ocean midlatitudes, especially in the SS simulation, while lower evaporation is located over the Eastern Mediterranean (Fig. 13c).

The ability of the different model configurations, as expected, gets weaker when simulating the single HPEs. In general, it is known that

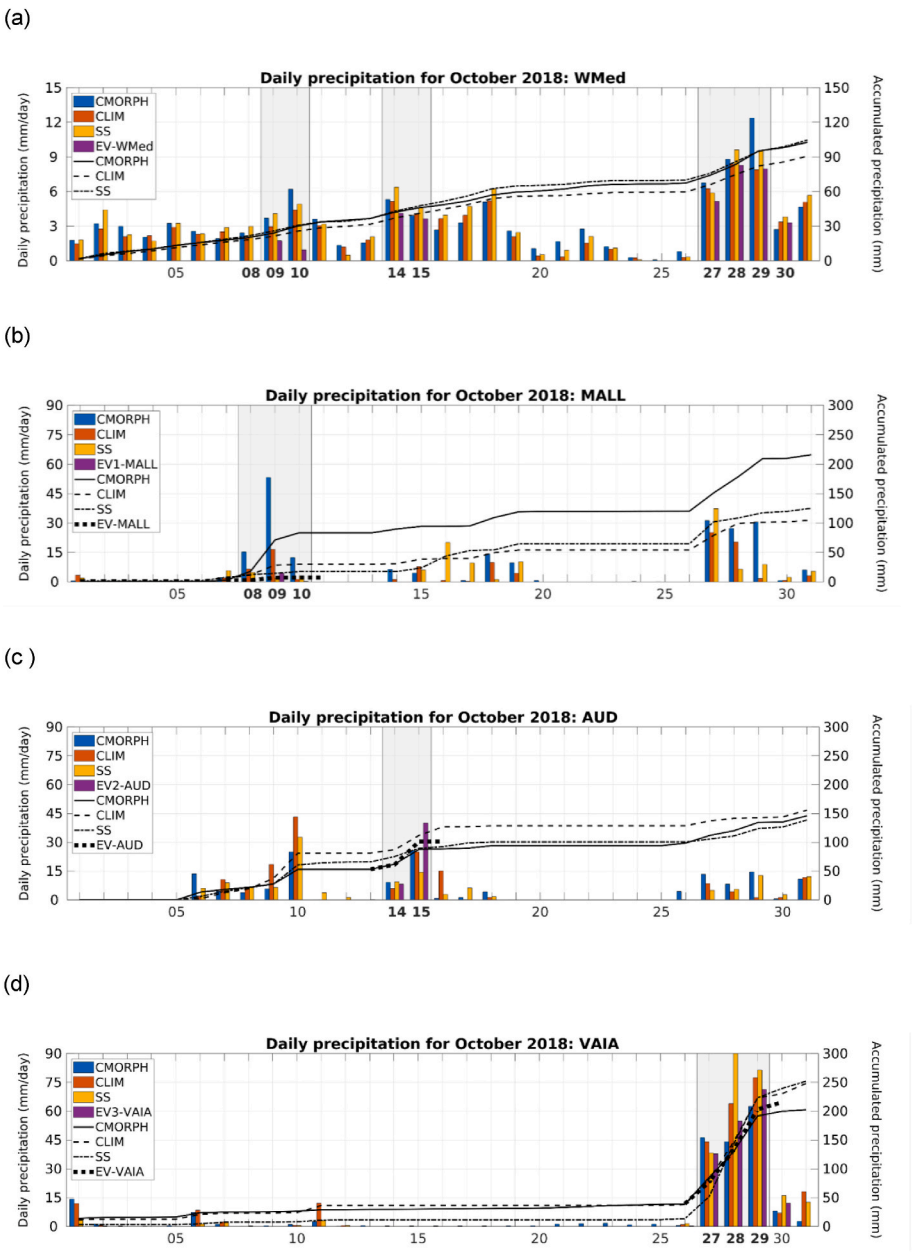

Fig. 12. Daily precipitation (bars) and total accumulated (lines) precipitation during October 2018 over (a) WMed, (b) MALL, (c) AUD and (d) VAIA from CMORPH (observations, blue bars and solid line), CLIM (RCM, red bars and dashed line), SS (seasonal RCM, yellow bars and dot-dashed line) and EV (NWP, purple bars and dotted line) at 2.8 km grid spacing except CLIM over WMed and VAIA (at 7 km) since the regions were not included in the innermost domain of 2.8 km. The duration of the corresponding event is marked by the grey shaded rectangles in the figures. In all cases a conservative upscaling to the coarser grid spacing of CMORPH is performed. (For interpretation of the references to colour in this figure legend, the reader is referred to the Web version of this article.)

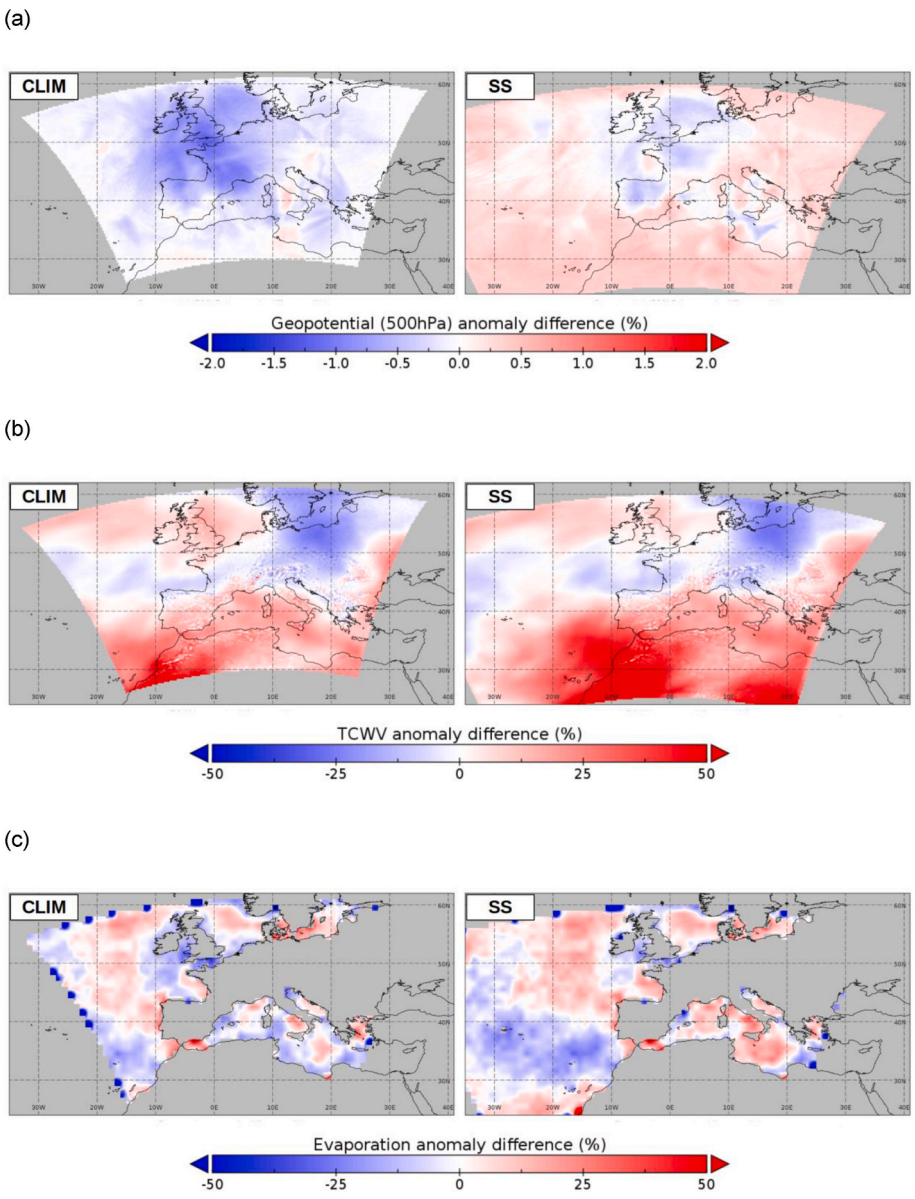

Fig. 13. For October 2018 and 7-km COSMO domains, (a) geopotential anomaly difference at 500 hPa and 5th percentile between CLIM and ERA5 (left) and SS and ERA5 (right), (b) mean TCWV anomaly difference between CLIM and ERA5 (left) and SS and ERA5 (right), and (c) mean evaporation anomaly difference between CLIM and OAFLUX (left) and SS and OAFLUX (right).

high-intensity short-duration convective events are in general not well reproduced by RCMs, despite their relevance, and the performance of NWP models highly depends on the specific model configuration and horizontal grid spacing (Khodayar et al., 2016). In this regard, the CLM and SS simulations (RCM configurations), as well as the event simulations (NWP configuration) capture the intense precipitation periods with different degrees of accuracy. The EV1-MALL shows very low predictability and is not accurately captured by any of the model simulations employed (Fig. 12b). This agrees with previous investigations pointing out the inability of predictive models to foresee this event (Lorenzo-Lacruz et al., 2019; Carrió et al., 2022). EV2-AUD and EV3-VAIA are better reproduced following the described higher-predictability of these cases (Caumont et al., 2021; Lorenzo-Lacruz et al., 2019). Even so, important differences are found between the simulations and the observed rainfall in these cases (Fig. 12c and d).

On an event scale, the simulations show relevant differences regarding the state of the atmosphere, which contributes to their general low predictability. The discrepancies among simulations and reference observations depend on the features of each HPE. To illustrate this analysis, the event showing the worst model representation, EV1-MALL, and the one with the best representation, EV3-VAIA, are discussed (Fig. 14). The latter, EV3-VAIA is generated due to a pronounced large-scale trough that slowly displaces eastward over the WMed generating an important water vapour advection over northern Italy (Fig. 14, right). The well-defined large-scale situation is well simulated by all model configurations. Discrepancies in the geopotential field can be noticed over the Iberian Peninsula, still far from the extreme precipitation affected area, in relation to the position of the upper-level low center. Also, the spatial distribution of daily mean TCWV over the Mediterranean Sea shows a moister environment, in relation to the strong moist flow towards the Alpine region, on the SS.

CLIM and EV simulations, which contribute to the precipitation overestimation of model simulations, of the same order, in comparison to the observations (Fig. 12d).

In contrast, the EV1-MALL is poorly represented in the simulations. The representations of the synoptic conditions show differences

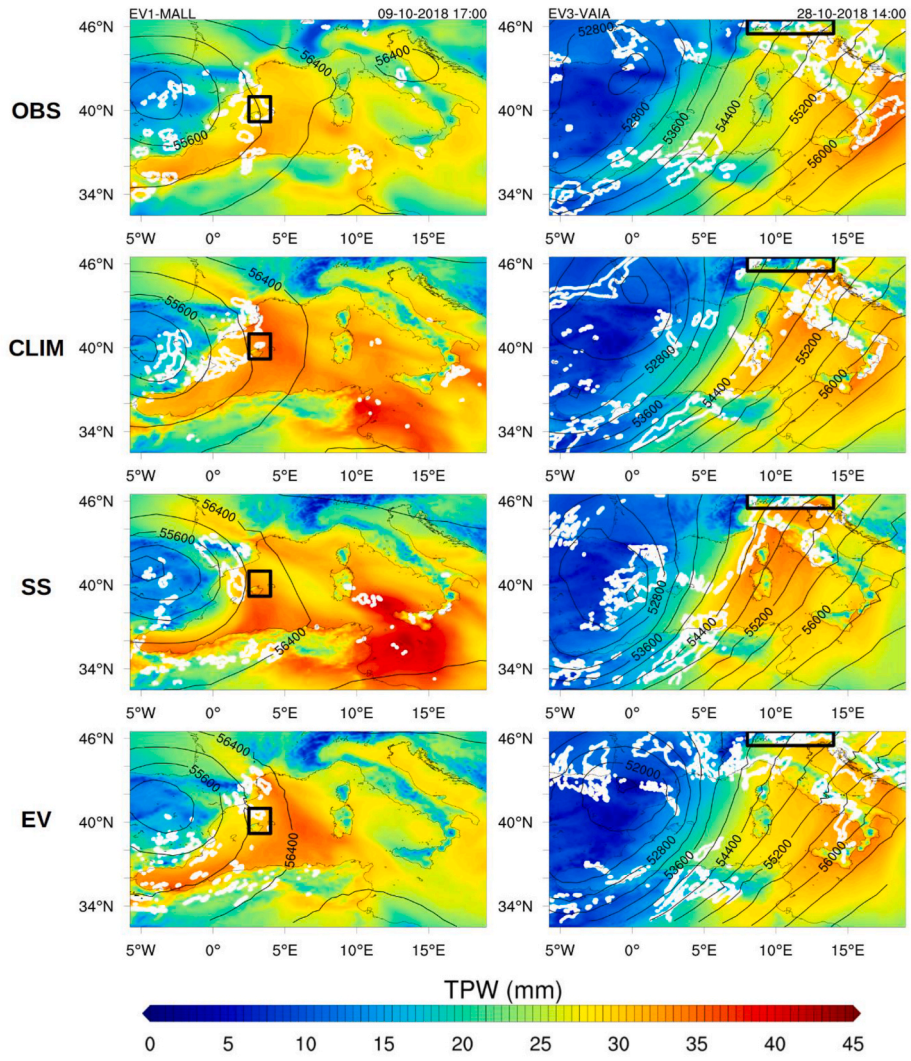

Fig. 14. Mean daily TCWV, hourly geopotential at 500 hPa (black lines) and precipitation (white lines) from (a) OBS, TCWV and geopotential from ERA5 and precipitation from CMORPH, (b) CLIM, (c) SS and (d) EV, for EV1-MALL (left) and EV3-VAIA (right). COSMO data (b,c and d) are obtained from the 7-km horizontal resolution domains.

associated with the location and intensity of the cut-off low over peninsular Spain, close to the Balearic Island, affected by the extreme event (Fig. 14, left). CLIM and SS simulate a more pronounced depression at 500 hPa than ERA5, generating a stronger gradient along eastern Spain, as well as a shift of its center toward west as also observed at the EV1-MALL simulation. Also, a different TCWV pattern is simulated in the CLIM and EV simulations suggesting that main water vapour advection occurs over the Gulf of Lion instead of over Mallorca, contributing to the underestimation of precipitation in those simulations, oppositely to the SS configuration that seems to capture TCWV distribution more accurately over the Balearic Islands despite significant differences in the area between Tunisia and Sicily.

6. Conclusions

In the present study, a comprehensive investigation of the underlying mechanisms leading to an extreme wet season in a well-known and recurrent heavy precipitation period for the western Mediterranean region is presented.

The Mediterranean region, every autumn, suffers heavy precipitation and flash flooding with catastrophic personal and socio-economic consequences. The autumn season of 2018, and particularly the October month, was particularly intense in terms of damaging extreme precipitation in the region, with millions of Euros and more than 20 personal losses. In this period, numerous heavy precipitation events affected the WMed, among them three historic extreme precipitation events defined the period. The first case occurred over the Balearic island of Palma de Mallorca in Spain on the 9 to 10 October 2018 (EV1: MALL, ES), on the 14 to 15 October, the Aude region in France (EV2: AUD, FR) was affected, and finally north and north-eastern Italy on the 27 to 29 October 2018 (EV3:Vaia, NI) lived a severe storm with over-damaging consequences.

In this investigation, the atmosphere and the ocean conditions in October 2018 are examined to identify large-scale factors, and their anomalies, contributing to the occurrence of the extreme wet period. Furthermore, the model representativity of the identified anomalies is analyzed across scales using climatological, seasonal, and event-based COSMO high-resolution model simulations.

Our results confirm that the atmosphere over the WMed region during October 2018 was moister than the nearly 40-year-period average investigated, practically for all the highest percentiles of total column atmospheric water vapour and specific humidity hourly anomalies up to the 500 hPa level. The observed moistest anomaly was identified at about 700 hPa, probably in relation to the moistening of the mid-tropospheric levels by the effect of the former hurricane Leslie (Caumont et al., 2021). Geopotential anomalies at the 300 and 500 hPa

levels were also exceptionally negative, indicating a frequent and over-averaged presence of cut-off lows over the region. Western Mediterranean SST was also clearly above the climatic mean from about April until the end of October. SST values exceeded the standard deviation in August and September leading to a huge energy accumulation in the WMed area. In relation to this, the presence of some peak evaporation events could be identified preceding and during October. In all three extreme events investigated, intense evaporation preceded the precipitation event period. The joint assessment of the evaporation vs SST monthly anomalies for the period 1982–2018 showed that October 2018 is not the most extreme period in terms of one or another which led to extreme wet seasons but the combination of relatively high values of both.

The relatively low predictability of the events, as pointed out in previous investigations using NWP configurations, was confirmed in this study across scales despite the use of high-resolution model simulations, about 3 km. Climate, seasonal and NWP simulations were confronted with observations regarding the monthly mean and event characteristics of the period. Results showed that while the accumulated precipitation for the October period was well represented by the CLIM and SS simulations, following an accurate representation of the large-scale synoptic forcing anomalies, the atmospheric water vapour content, and the SST positive anomaly, on the event scale simulations relevant discrepancies were identified. Differences at the location and intensity of the cut-off lows and particularly at the atmospheric moisture field distribution turned out to be key to obtain an accurate representation of the amount, timing, and location of the event-based extreme precipitation.

This study provides a comprehensive view of one of the most extreme precipitation periods in the Western Mediterranean region in the last decades contributing to better understanding the underlying mechanisms leading to extreme wet seasons and their model representativity. Findings from this investigation let us conclude that it is the synergetic occurrence of ocean and atmospheric anomalies, which creates the favourable environment for an extreme precipitation season defined by high-intense precipitation events, rather than the single maximum or extreme anomalies from each one of the investigated factors.

Our results contribute to researchers' goal of improving the capability of mesoscale models to better represent extreme precipitation seasons and events, additionally aiding forecasters to evaluate the adequate information from other sources when the usual forecasting tools fail. It will be of great interest to evaluate if the conditions described in this study are common to all autumn seasons/months characterized as "extreme seasons/periods". As such, this will be a future effort of the authors. Furthermore, key features as the correct representation of the former hurricane Leslie, in this case in terms of its contribution to the atmospheric moisture distribution during the study period, suggests the need to further invest in the assimilation of station data over land and sea in high-resolution convection permitting models.

7. Authorship contribution statement

All authors contributed to the discussion, drafting and refinement of this manuscript. In particular, the first author, SK conceived the study and was in charge of the overall direction and planning, FP contributed to the analysis of the oceanic anomalies, JAV contributed to the analysis of the large-scale atmospheric conditions, PB contributed to the analysis of the model simulations representativity of the analyzed conditions and FE contributed with the performance of the event scale model simulations.

Declaration of competing interest

The authors declare that they have no conflict of interest.

Acknowledgements

The Precipitation - CMORPH Climate Data Record (CDR) used in this study was acquired from the NOAA National Centers for Environmental Prediction (NCEP). This CDR was developed by Pingping Xie of NOAA-CPC, Robert Joyce, Shaorong Wu Soo-Hyun Yoo, Yelena Yarosh, Fengying Sun, and Roger Lin of Innovim, LLC. ERA5 data (Hersbach et al., 2018) was downloaded from the Copernicus Climate Change Service (C3S) Climate Data Store. The results contain modified Copernicus Climate Change Service information 2020. Neither the European Commission nor ECMWF is responsible for any use that may be made of the Copernicus information or data it contains. The evaporation analysis is based upon the WHOI OAFlux datasets supported by the NOAA's Global Ocean Monitoring and Observing (GOMO) Program and NASA's Making Earth System Data Records for Use in Research Environments (MEaSUREs) Program. Data were partially generated using Copernicus Climate Change Service information [2021]. SST daily data available from National Centers for Environmental Information. 2016. GHRSST Level 4 AVHRR_OI Global Blended Sea Surface Temperature Analysis (GDS version 2) from NCEI. Ver. 2.0. PO.DAAC, CA, USA. Dataset last accessed 2021-06-01 at https://doi.org/10.5067/GHAAO-4BC02. "The Group for High Resolution Sea Surface Temperature (GHRSST) AVHRR_OI Global Blended Sea Surface Temperature Analysis (GDS version 2) data were obtained from the NASA EOSDIS Physical Oceanography Distributed Active Archive Center (PO.DAAC) at the Jet Propulsion Laboratory, Pasadena, CA (https://doi.org/10.5067/GHGMR-4FJ01)." COSMO simulations were performed at the German Climate Computing Center (DKRZ, Hamburg) and the Steinbuch Centre for Computing (SCC) of the Karlsruhe Institute of Technology (KIT). This research work was partially funded by the Bundesministerium für Bildung und Forschung (BMBF; German Federal Ministry of Education and Research) project PREMIUM 01LN1319A. We thank Sebastian Helgert (KIT) and Alberto Caldas-Álvarez (KIT) for assistance with the COSMO model and helpful discussions. We also would like to thank Belén Rico for her contribution in the final correction of the manuscript. The contribution of Pau Benetó Vallés was supported by the project IMAGINA-PROMETEO (PROMETEO/2019/110) of Generalitat Valenciana. The Mediterranean Centre for Environmental Studies (CEAM) is partly supported by Generalitat Valenciana. The contribution of the first author Samira Khodayar Pardo was supported by the project MED-EXTREME, program Generació Talent of Generalitat Valenciana (CIDEGENT/2018/017).

Appendix A. Supplementary data

Supplementary data to this article can be found online at https://doi.org/10.1016/j.wace.2022.100493.

References

Baldauf, M., Seifert, A., Förstner, J., Majewski, D., Raschendorfer, M., 2011. Operational convective-scale numerical weather prediction with the COSMO model: description and sensitivities. Mon. Weather Rev. 139, 3887–3905.

Banzon, V., Smith, T.M., Mike Chin, T., Liu, C., Hankins, W., 2016. A long-term record of blended satellite and in situ sea-surface temperature for climate monitoring, modeling and environmental studies. Earth Syst. Sci. Data 8 (1), 165–176. https://doi.org/10.5194/essd-8-165-2016.

Buzzi, A., Davolio, S., Malguzzi, P., Drofa, O., Mastrangelo, D., 2014. Heavy rainfall episodes over Liguria in autumn 2011: numerical forecasting experiments. Nat. Hazards Earth Syst. Sci. 14 (6), 1325–1340. https://doi.org/10.5194/nhess-14-1325-2014.

Carrió, D.S., Jansà, A., Homar, V., Romero, R., Rigo, T., Ramis, C., Hermoso, A., Maimó, A., 2022. Exploring the benefits of a Hi-EnKF system to forecast an extreme weather event. The 9th October 2018 catastrophic flash flood in Mallorca. Atmos. Res. 265 https://doi.org/10.1016/j.atmosres.2021.105917.

Caumont, O., Mandement, M., Bouttier, F., Eeckman, J., Brossier, C.L., Lovat, A., Nuissier, O., Laurantin, O., 2021. The heavy precipitation event of 14-15 October 2018 in the Aude catchment: a meteorological study based on operational numerical weather prediction systems and standard and personal observations. Nat. Hazards Earth Syst. Sci. 21 (3), 1135–1157. https://doi.org/10.5194/nhess-21-1135-2021.

Davolio, S., Della Fera, S., Laviola, S., Miglietta, M.M., Levizzani, V., 2020. Heavy precipitation over Italy from the Mediterranean storm "Vaia" in October 2018:

assessing the role of an atmospheric river. Mon. Weather Rev. 148 (9), 3571–3588. https://doi.org/10.1175/MWR-D-20-0021.1.
Delrieu, G., Ducrocq, V., Gaume, E., Nicol, J., Payrastre, O., Yates, E., Kirstetter, P.E., Andrieu, H., Ayral, P.A., Bouvier, C., Creutin, J.D., Livet, M., Anquetin, S., Lang, M., Neppel, L., Obled, C., Parent-Du-Châtelet, J., Saulnier, G.M., Walpersdorf, A., Wobrock, W., 2005. The catastrophic flash-flood event of 8-9 September 2002 in the Gard Region, France: a first case study for the Cévennes-Vivarais Mediterranean Hydrometeorological Observatory. J. Hydrometeorol. 6 (1), 34–52. https://doi.org/10.1175/JHM-400.1.
Dobrovičová, S., Dobrovič, R., Dobrovič, J., 2015. The economic impact of floods and their importance in different regions of the world with emphasis on Europe. Procedia Econ. Finance 34 (15), 649–655. https://doi.org/10.1016/s2212-5671(15)01681-0.
Doms, G., Förstner, J., Heise, E., Herzog, H.-J.-, Raschendorfer, M., Schrodin, R., Reinhardt, T., Vogel, G., 2013. A description of the nonhydrostatic regional model LM. Part II: Physical parameterization. Tech. Rep., Deutscher Wetterdienst, Offenbach, Germany [Available online at. https://www.cosmo-model.org/content/model/documentation/core/cosmo_physics_5.00.pdf, 156.
Duffourg, F., Ducrocq, V., 2011. Origin of the moisture feeding the heavy precipitating systems over southeastern France. Nat. Hazards Earth Syst. Sci. 11 (4) https://doi.org/10.5194/nhess-11-1163-2011.
Durack, P.J., Wijffels, S.E., Matear, R.J., 2012. Ocean salinities reveal strong global water cycle intensification during 1950 to 2000. Science 336 (6080), 455–458. https://doi.org/10.1126/science.1212222.
Ehmele, F., Barthlott, C., Corsmeier, U., 2015. The influence of Sardinia on Corsican rainfall in the western Mediterranean Sea: a numerical sensitivity study. Atmos. Res. 153, 451–464. https://doi.org/10.1016/j.atmosres.2014.10.004.
Ferreira, R.N., 2021. Cut-off lows and extreme precipitation in Eastern Spain: current and future climate. Atmosphere 12 (7), 835. https://doi.org/10.3390/atmos12070835.
Ferretti, R., Low-Nam, S., Rotunno, R., 2000. Numerical simulations of the piedmont flood of 4–6 November 1994. Tellus Dyn. Meteorol. Oceanogr. 52 (2), 162–180. https://doi.org/10.1034/j.1600-0870.2000.00992.x.
Flaounas, E., Röthlisberger, M., Boettcher, M., Sprenger, M., Wernli, H., 2021. Extreme wet seasons – their definition and relationship with synoptic-scale weather systems. Weather Clim. Dyn. 2 (1), 71–88. https://doi.org/10.5194/wcd-2-71-2021.
Giovannini, L., Davolio, S., Zaramella, M., Zardi, D., Borga, M., 2021. Multi-model convection-resolving simulations of the October 2018 Vaia storm over Northeastern Italy. Atmos. Res. 253, 105455 https://doi.org/10.1016/j.atmosres.2021.105455.
Hersbach, H., Bell, B., Berrisford, P., Biavati, G., Horányi, A., Muñoz Sabater, J., Nicolas, J., Peubey, C., Radu, R., Rozum, I., Schepers, D., Simmons, A., Soci, C., Dee, D., Thépaut, J.-N., 2018. ERA5 hourly data on pressure levels from 1979 to present. Copernicus Climate Change Service (C3S) Climate Data Store (CDS). https://doi.org/10.24381/cds.bd0915c6, 15-04-2021 to 15-08-2021.
Hersbach, H., Bell, B., Berrisford, P., Hirahara, S., Horányi, A., Muñoz-Sabater, J., Nicolas, J., Peubey, C., Radu, R., Schepers, D., Simmons, A., Soci, C., Abdalla, S., Abellan, X., Balsamo, G., Bechtold, P., Biavati, G., Bidlot, J., Bonavita, M., Thépaut, J.N., 2020. The ERA5 global reanalysis. Q. J. R. Meteorolog. Soc. 146 (730), 1999–2049. https://doi.org/10.1002/qj.3803.
Homar, V., Romero, R., Ramis, C., Alonso, S., 2002. Numerical study of the October 2000 torrential precipitation event over eastern Spain: analysis of the synoptic-scale stationarity. Ann. Geophys. 20 (12), 2047–2066. https://doi.org/10.5194/angeo-20-2047-2002.
Insua-Costa, D., Lemus-Cánovas, M., Miguez-Macho, G., Llasat, M.C., 2021. Climatology and ranking of hazardous precipitation events in the western Mediterranean area. Atmos. Res. 255, 105521 https://doi.org/10.1016/j.atmosres.2021.105521.
Jacobsen, I., Heise, E., 1982. A new economic method for the computation of the surface temperature in numerical models. Contrib. Atmos. Phys. 55, 128–142.
Joyce, R.J., Janowiak, J.E., Arkin, P.A., Xie, P., 2004. CMORPH: a method that produces global precipitation estimates from passive microwave and infrared data at high spatial and temporal resolution. J. Hydrometeorol. 5 (3), 487–503. https://doi.org/10.1175/1525-7541(2004)005<0487:CAMTPG>2.0.CO;2.
Khodayar, S., Fosser, G., Berthou, S., Davolio, S., Drobinski, P., Ducrocq, V., Ferretti, R., Nuret, M., Pichelli, E., Richard, E., Bock, O., 2016. A seamless weather–climate multi-model intercomparison on the representation of a high impact weather event in the western Mediterranean: HyMeX IOP12. Q. J. R. Meteorol. Soc. 142, 433–452. https://doi.org/10.1002/qj.2700.
Khodayar, S., Kalthoff, N., Kottmeier, C., 2018a. Atmospheric conditions associated with heavy precipitation events in comparison to seasonal means in the western mediterranean region. Clim. Dynam. 51 (3) https://doi.org/10.1007/s00382-016-3058-y.
Khodayar, S., Czajka, B., Caldas-Alvarez, A., Helgert, S., Flamant, C., di Girolamo, P., Bock, O., Chazette, P., 2018b. Multi-scale observations of atmospheric moisture variability in relation to heavy precipitating systems in the northwestern Mediterranean during HyMeX IOP12. Q. J. R. Meteorol. Soc. 144 (717), 2761–2780. https://doi.org/10.1002/qj.3402.
Khodayar, S., Davolio, S., di Girolamo, P., Lebeaupin Brossier, C., Flaounas, E., Fourrie, N., Lee, K.-O., Ricard, D., Vie, B., Bouttier, F., Caldas-Alvarez, A., Ducrocq, V., 2021. Overview towards improved understanding of the mechanisms leading to heavy precipitation in the western Mediterranean: lessons learned from HyMeX. Atmos. Chem. Phys. 21 (22) https://doi.org/10.5194/acp-21-17051-2021.
Kron, W., Eichner, J., Kundzewicz, Z.W., 2019. Reduction of flood risk in Europe – reflections from a reinsurance perspective. J. Hydrol. 576 (April), 197–209. https://doi.org/10.1016/j.jhydrol.2019.06.050.
Llasat, M.C., Llasat-Botija, M., Prat, M.A., Porcú, F., Price, C., Mugnai, A., Lagouvardos, K., Kotroni, V., Katsanos, D., Michaelides, S., Yair, Y., Savvidou, K., Nicolaides, K., 2010. High-impact floods and flash floods in Mediterranean countries: the FLASH preliminary database. Adv. Geosci. 23, 47–55. https://doi.org/10.5194/adgeo-23-47-2010.
Llasat, M.C., 2021. Floods evolution in the mediterranean region in a context of climate and environmental change. Geogr. Res. 47 (1) https://doi.org/10.18172/cig.4897.
Lorenzo-Lacruz, J., Amengual, A., Garcia, C., Morán-Tejeda, E., Homar, V., Maimó-Far, A., Hermoso, A., Ramis, C., Romero, R., 2019. Hydro-meteorological reconstruction and geomorphological impact assessment of the October 2018 catastrophic flash flood at Sant Llorenç, Mallorca (Spain). Nat. Hazards Earth Syst. Sci. 19 (11), 2597–2617. https://doi.org/10.5194/nhess-19-2597-2019.
Louis, J.F., 1979. A parametric model of vertical eddy fluxes in the atmosphere. Boundary-Layer Meteorol. 17 (2), 187–202. https://doi.org/10.1007/BF00117978.
Mandement, M., Caumont, O., 2021. A numerical study to investigate the roles of former Hurricane Leslie, orography and evaporative cooling in the 2018 Aude heavy-precipitation event. Weather Clim. Dyn. 2 (3), 795–818. https://doi.org/10.5194/wcd-2-795-2021.
Mariotti, A., 2010. Recent changes in the mediterranean water cycle: a pathway toward long-term regional hydroclimatic change? J. Clim. 23 (6), 1513–1525. https://doi.org/10.1175/2009JCLI3251.1.
Martínez, C., Campins, J., Jansà, A., Genovés, A., 2008. Heavy rain events in the Western Mediterranean: an atmospheric pattern classification. Adv. Sci. Res. 2 (1), 61–64. https://doi.org/10.5194/asr-2-61-2008.
Mellor, G.L., Yamada, T., 1974. A hierarchy of turbulence closure models for planetary boundary layers. J. Atmos. Sci. 31 (7), 1791–1806. https://doi.org/10.1175/1520-0469(1974)031<1791:ahotcm>2.0.co;2.
Michaelides, S., Karacostas, T., Sánchez, J.L., Retalis, A., Pytharoulis, I., Homar, V., Romero, R., Zanis, P., Giannakopoulos, C., Bühl, J., Ansmann, A., Merino, A., Melcón, P., Lagouvardos, K., Kotroni, V., Bruggeman, A., López-Moreno, J.I., Berthet, C., Katragkou, E., Tymvios, F., Hadjimitsis, D.G., Mamouri, R.E., Nisantzi, A., 2018. Reviews and perspectives of high impact atmospheric processes in the Mediterranean. Atmos. Res. 208, 4–44. https://doi.org/10.1016/j.atmosres.2017.11.022.
Nuissier, O., Joly, B., Joly, A., Ducrocq, V., Arbogast, P., 2011. A statistical downscaling to identify the large-scale circulation patterns associated with heavy precipitation events over southern France. Q. J. R. Meteorol. Soc. 137 (660) https://doi.org/10.1002/qj.866.
Paprotny, D., Sebastian, A., Morales-Nápoles, O., Jonkman, S.N., 2018. Trends in flood losses in Europe over the past 150 years. Nat. Commun. 9 (1) https://doi.org/10.1038/s41467-018-04253-1.
Pastor, F., Estrela, M.J., Peñarrocha, D., Millán, M.M., 2001. Torrential rains on the Spanish Mediterranean Coast: modeling the effects of the sea surface temperature. J. Appl. Meteorol. 40 (7), 1180–1195. https://doi.org/10.1175/1520-0450(2001)040<1180:TROTSM>2.0.CO;2.
Pastor, F., Gómez, I., Estrela, M.J., 2010. Numerical study of the October 2007 flash flood in the Valencia region (Eastern Spain): the role of orography. Nat. Hazards Earth Syst. Sci. 10 (6), 1331–1345. https://doi.org/10.5194/nhess-10-1331-2010.
Pastor, F., Valiente, J.A., Estrela, M.J., 2015. Sea surface temperature and torrential rains in the Valencia region: modelling the role of recharge areas. Nat. Hazards Earth Syst. Sci. 15 (7), 1677–1693. https://doi.org/10.5194/nhess-15-1677-2015.
Pastor, F., Valiente, J.A., Khodayar, S., 2020. A warming Mediterranean: 38 years of increasing sea surface temperature. Rem. Sens. 12 (17), 2687. https://doi.org/10.3390/RS12172687.
Pastor, F., Valiente, J.A., Palau, J.L., 2018. sea surface temperature in the mediterranean: trends and spatial patterns (1982–2016). Pure Appl. Geophys. 175 (11), 4017–4029. https://doi.org/10.1007/s00024-017-1739-z.
Pinto, J.G., Ulbrich, S., Boni, G., Parodi, A., Rudari, R., Ulbrich, U., 2013. Identification and ranking of extraordinary rainfall events over Northwest Italy: the role of Atlantic moisture. J. Geophys. Res. Atmos. 118, 2085–2097. https://doi.org/10.1002/jgrd.50179.
Reynolds, R.W., Smith, T.M., Liu, C., Chelton, D.B., Casey, K.S., Schlax, M.G., 2007. Daily high-resolution-blended analyses for sea surface temperature. J. Clim. 20 (22), 5473–5496. https://doi.org/10.1175/2007JCLI1824.1.
Ricard, D., Ducrocq, V., Auger, L., 2012. A climatology of the mesoscale environment associated with heavily precipitating events over a northwestern Mediterranean area. J. Appl. Meteorol. 51 (3), 468–488. https://doi.org/10.1175/JAMC-D-11-017.1.
Ritter, B., Geleyn, J.F., 1992. A comprehensive radiation scheme for numerical weather prediction models with potential applications in climate simulations. Mon. Weather Rev. 120 (2), 303. https://doi.org/10.1175/1520-0493(1992)120<0303:ACRSFN>2.0.CO;2.
Rockel, B., Will, A., Hense, A., 2008. The regional climate model COSMO-CLM (CCLM). Meteorol. Z. 17 (4), 347–348. https://doi.org/10.1127/0941-2948/2008/0309.
Romero, R., Ramis, C., Guijarro, J.A., 1999. Daily rainfall patterns in the Spanish Mediterranean area: an objective classification. Int. J. Climatol. 19 (1), 95–112. https://doi.org/10.1002/(SICI)1097-0088(199901)19:1<95::AID-JOC344>3.0.CO;2-S.
Scoccimarro, E., Gualdi, S., Bellucci, A., Zampieri, M., Navarra, A., 2016. Heavy precipitation events over the Euro-Mediterranean region in a warmer climate: results from CMIP5 models. Reg. Environ. Change 16 (3), 595–602. https://doi.org/10.1007/s10113-014-0712-y.
Skliris, N., Zika, J.D., Nurser, G., Josey, S.A., Marsh, R., 2016. Global water cycle amplifying at less than the Clausius-Clapeyron rate. Sci. Rep. 6, 38752 https://doi.org/10.1038/srep38752.
Swiss, Re, 2020. Catástrofes Naturales en Tiempos de Acumulación Económica y Riesgos Climáticos. Informes Sigma 2. Available online: https://www.swissre.com/institute/research/sigma-research/sigma-2020-02.html.

Tiedtke, M., 1989. A comprehensive mass flux scheme for cumulus parameterization in large-scale models. Mon. Weather Rev. 117 (8), 1779–1799. https://doi.org/10.1175/1520-0493(1989)117<1779:ACMFSF>2.0.CO;2.

Tramblay, Y., Somot, S., 2018. Future evolution of extreme precipitation in the Mediterranean. Clim. Change 151 (2). https://doi.org/10.1007/s10584-018-2300-5.

Yu, L., Weller, R.A., 2007. Objectively analyzed air-sea heat fluxes for the global ice- free oceans (1981-2005). Bull. Am. Meteorol. Soc. 88 (4), 527–539. https://doi.org/10.1175/BAMS-88-4-527.